Hindawi
International Journal of Aerospace Engineering
Volume 2022, Article ID 6358188, 18 pages
https://doi.org/10.1155/2022/6358188

Research Article

Satellite In-Orbit Secondary Collision Risk Assessment

Haicheng Tao, Xueke Che, Qinyu Zhu, and XinHong Li

Space Engineering University, Beijing 101416, China

Correspondence should be addressed to XinHong Li; 13366159269@189.cn

Received 15 January 2022; Accepted 24 March 2022; Published 2 May 2022

Academic Editor: Yue Wang

The massive mega constellation of satellites will have a significant impact on global space safety. With Starlink as an example, this paper is aimed at assessing the risk of in-orbit collision, analyzing the probability of collision in orbit in its natural operating state, and forecasting the probability of secondary collision between the collision-generated short-term debris cloud and satellites in the same orbit. The mass, size, velocity, and direction of space debris in a particular orbit of Starlink satellite are calculated based on the MASTER-8 model, and the shape characteristics of the Starlink satellite are added to the model to determine the probability of a Starlink satellite colliding with space debris in that orbit. A modified spacecraft impact disintegration model then is used to calculate the collision results and estimate the collision threat level of the short-term debris cloud formed by the Starlink satellite after its destruction to satellites in the same orbit. The results indicate that the collision probability of Starlink satellite in orbit natural operation exceeds the red warning threshold 10^{-4} that the satellite disintegration after the first collision will generate 14088 pieces of debris over 1 cm, of which 4092 debris are potentially dangerous to other spacecraft, and that the collision probability to a satellite in the same orbit exceeds the red warning threshold of 10^{-4} within 30 minutes, implying that collision avoidance needs to be improved.

1. Introduction

Many countries are developing their plans for mega constellations [1], and the sheer scale of which poses a threat to space safety. The Federal Communications Commission (FCC) stated in an order and authorization issued on April 27, 2021, that it would allow SpaceX to move 2,814 satellites from 1,100 to 1,300 kilometres to 540 to 570 kilometres from orbit. This orbital range is identical to that of the existing fleet of around 1,350 satellites, and SpaceX intends to eventually launch 42,000 Starlink satellites to build a global broadband network [1] According to OneWeb, the completed OneWeb constellation will consist of 720 satellites distributed across 40 orbital planes, with 18 satellites in each orbital plane. The constellation will operate at an altitude of 1,200 kilometres [2]. It can be expected that the entire low-orbit region will be densely packed with satellites, forming a "sea of satellites." With low-orbit orbital space debris denser and faster, the probability of collision is higher than at other orbital altitudes, and the large number will also increase the probability of collision, having a significant impact on international space resources. At the same time, for the future docking launch of the space station after the completion of the network, Starlink satellites will be located at 335-346 km and 550 km, respectively, which is extremely unfavourable for the space launch; the launch window will be greatly reduced, the future launch mission will be more difficult, and the mission requirements will be increased [3]. In a nutshell, the launch window will be significantly limited, resulting in more challenging and demanding missions in the future.

The European Space Agency (ESA) manoeuvres an Earth science satellite, Aeolus, in 2019 to avoid a potential collision with the Starlink-44 satellite [4]. The Hubble Space Telescope, which orbits at a similar altitude of approximately 640 kilometres, may also collide with the Starlink satellite, which flew too close to the Chinese space station twice, according to a document presented by China to the UN space agency in December. The first incident occurred on July 1, and the second was on October 21, 2021, when the Chinese space station was forced to make manoeuvres to avoid collision [5]. Numerous other spacecraft in LEO are

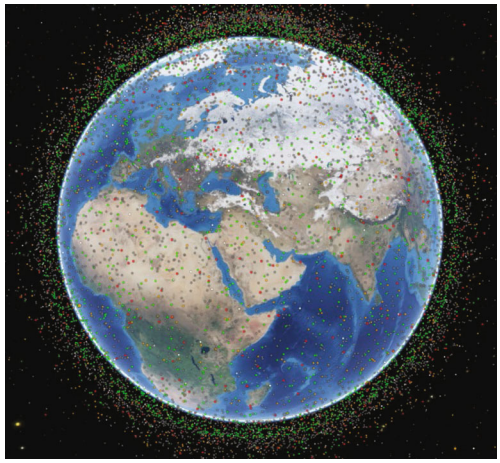

Figure 1: Low orbit space debris distribution [8]

also affected by Starlink satellites in terms of orbital safety. The need for orbital transfer to avoid collisions consumes propellant, i.e., the lifetime of the satellite is reduced, and also poses a challenge for normally operating satellites in the same orbit.

Liou et al. modelled the evolution of the LEO debris population over 10 cm in size over the next 100-200 years, estimating that even with a 50% compliance mitigation rate, the LEO debris population could double in 200 years [6], and the debris population is increasing as a result of continued launch activity and spontaneous space collisions and breakups. Atmospheric drag alone is not sufficient to stop this trend. With an increase in the number of objects in orbit, the likelihood of collisions grows proportionately [6]. Starlink satellites are subjected to several close (i.e., within a few kilometres) flybys each day [7]. Each close encounter represents a potential collision, and each collision produces more debris, increasing the likelihood of future collisions. According to some reports, when the number of objects in orbit is high enough, a self-sustaining collision cascade process dubbed the Kessler syndrome will develop [7]. The probability of collision between a massive amount of orbital debris and an equally large number of mega constellations would reach a frightening level, thus dramatically increasing the safety threat to space. Figure 1 shows the distribution of space debris in extraterrestrial orbit. Low-orbit space debris is already extremely dense, threatening the in-orbit satellites.

For collisions in mega constellations, Anselmo and Pardini argue that unchecked growth in the number of constellation satellites can increase the average collision rate of catalogued objects in near-Earth orbit by 10% [9]. Radtke et al. argue that for the OneWeb constellation, debris larger than 3 cm would cause catastrophic collisions with OneWeb-sized satellites that such a mega constellation would have a 35% probability of catastrophic collisions over its lifetime, and that debris clouds from satellite collisions would lead to an approximately 34% increase in the constellation's debris flux after 10 years [2]. Boley and Byers concluded that there is a 92% possibility of one or more debris collisions between uncatalogued debris and Starlink satellites at a 550-kilometre altitude within a year [10].

With such a dense constellation of satellites, secondary collisions may occur after the collision and are more difficult to predict and prevent due to the brief duration of the event. Then, it will be more dangerous if the mega constellation collides with space debris, considering the secondary accident scenario because the orbital parameters of the thousands of pieces of debris generated by the collision are unknown and can be accurately measured only after the event. It is also difficult to estimate the number of satellites requiring orbit corrections if only Starlink satellites at adjacent orbital altitudes are considered. Research on secondary collisions is still weak, and it is impossible to know how secondary collisions of mega constellations will actually affect space safety. The purpose of this paper is to investigate the secondary collisions of the constellation, to assess the probability of secondary collisions in the short-term debris clouds generated by Starlink satellites following one collision with space debris and to analyze the safety risks to low-orbit space posed by the constellation.

2. Calculation Process and Model

To calculate the collision probability with space debris, the Starlink-61 satellite orbit with NORAD CAT ID 44249 is chosen, and the mass, size, and velocity flux of space debris, as well as the azimuth and elevation fluxes of space debris, are calculated. The disintegration state is estimated based on the collision scenario to derive the mass, size, and velocity distribution of the disintegrated debris cloud, and the satellite is made to cross the debris cloud to get the probability of collision between the debris cloud and the satellite in the same orbit. Figure 2 is the flow chart of the calculation model.

2.1. Orbital Debris Distribution and Collision Probability Model. The flux calculation of the MASTER-8 model employs a method similar to that used in the gas dynamics theory, where the space debris passes through the particle-filled space environment as if it were swept through a space container filled with static gas, called a "bin," as follows. As shown below in Figure 3, the Earth's orbital space is divided into an infinite number of similar spatial containers, where Δh denotes the container height, $\Delta\alpha$ denotes the container longitude span, and $\Delta\delta$ denotes the latitude span.

Equation (1) can be applied to determine the average number of collisions n [2].

$$n = F \times A_c \times T. \tag{1}$$

F is the flux, T is the time frame, and A_c is the cross-sectional area of the collision, which in this case is the cross-section area of the Starlink satellite in orbit.

From the average number of collisions n, the collision probability can be calculated using Poisson statistics

$$P_{i=m} = \frac{n^m}{m!} e^{-n}. \tag{2}$$

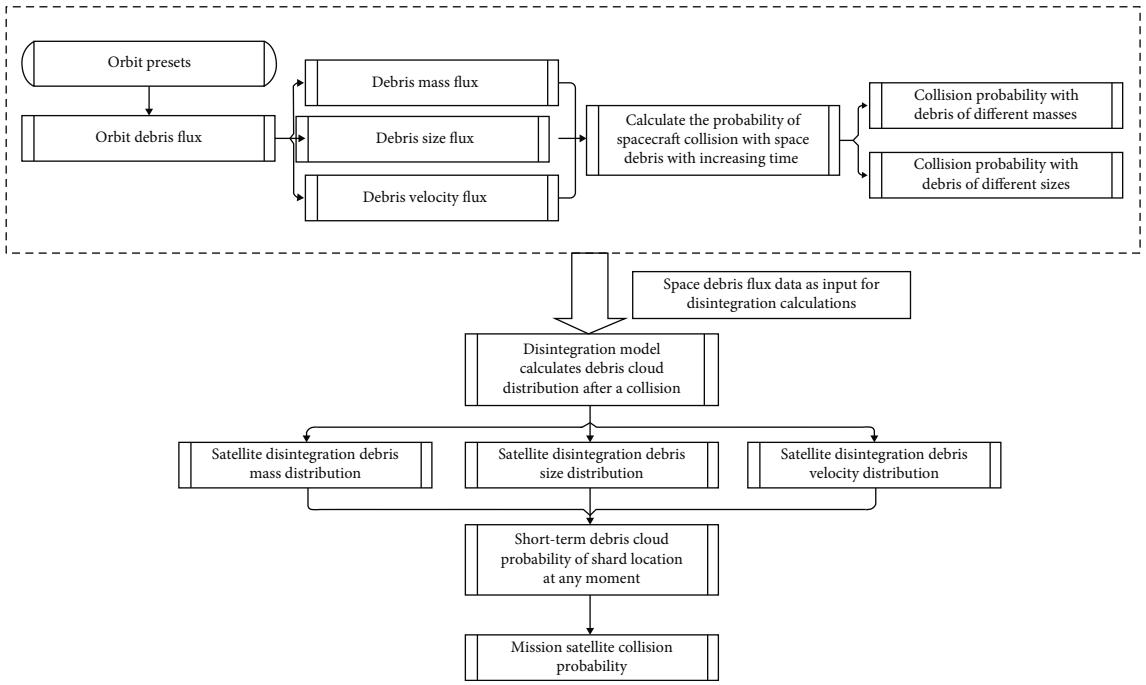

Figure 2: Computational model flow chart.

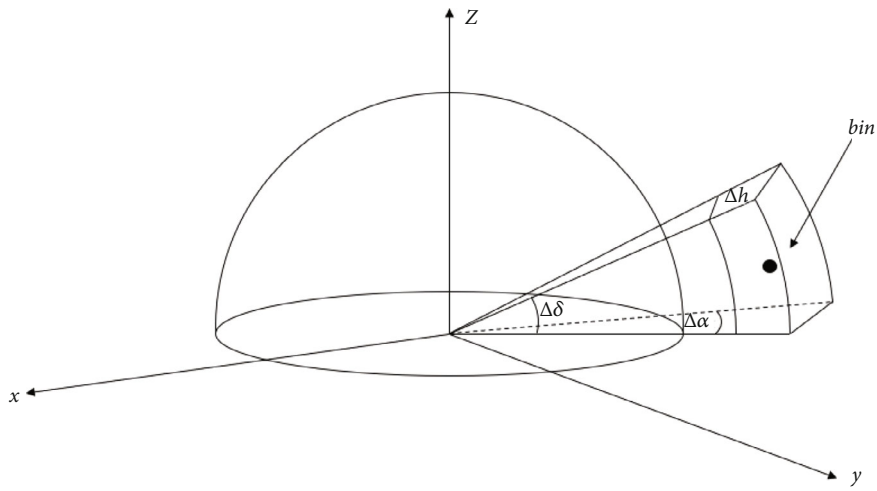

Figure 3: Bin's spatial pattern.

2.2. Space Collision Breakup Model. The Space Collision Breakup Model (SCBM) is used to forecast the collision results, and it outperforms the early impact breakup model, the Ballelle model, and NASA's LEGEND model [11].

2.2.1. Debris Mass Distribution Model. In describing the impact destruction of a target, it is necessary to identify whether it is partially or completely disintegrated. For this purpose, the model defines an impact disintegration limit, i.e., the critical specific energy $\widehat{E}_P^*$; when the actual energy ratio $\widehat{E}_P \geq \widehat{E}_P^*$, the target is completely disintegrated, and it is a catastrophic impact; otherwise, the target is only partially disintegrated. According to the characteristics of the Starlink satellite structure, the disintegration limit is defined as $\widehat{E}_P^* = 40J/g$ [2], and Equation (3) is the actual energy ratio.

$$\widehat{E}_P = \frac{m_p v^2}{2m_t}. \tag{3}$$

m_p is the debris mass, m_t is the object mass, v is the debris velocity, and the following Equation (4) is used to represent postimpact mass distribution [12]:

$$N(m) = A\left(\frac{m}{m_{\text{tot}}}\right)^{-B}. \tag{4}$$

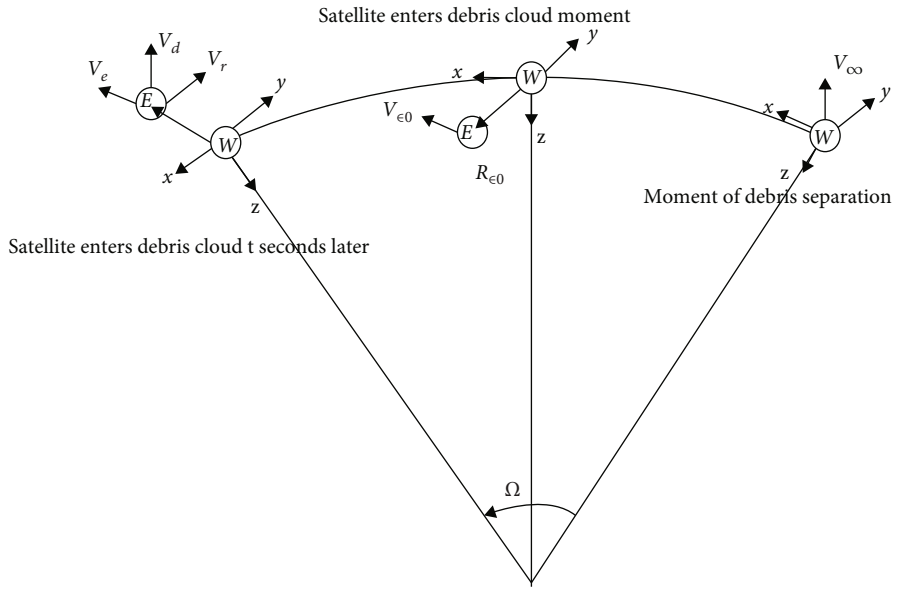

Figure 4: Position-velocity relationship between satellite E and debris cloud centre W.

m is the distributed mass, $N(m)$ is the mass of debris greater than or equal to m in the impact-generated debris, and m_{tot} is the mass of the object before disintegration. The value of the power factor B fluctuates depending on the degree of impact. Proportionality factor A depends on B.

2.2.2. Debris Size Distribution Model. The size distribution represents the number of fragments of various sizes produced after impact. The SCBM model is improved from the NASA model in terms of the size distribution function by taking fragment velocity, impact kinetic energy, and other factors into account. It has wider applicability, $N(L_c)$ represents the number of debris of size greater than or equal to a given size after impact [13].

$$N(L_c) = A\left(\frac{5.9819L_c^{2.28}}{m_{\text{tot}}}\right)^{-B} = 5.9819^{-B}m_{\text{tot}}^{B}AL_c^{-2.28B}. \quad (5)$$

L_c is the feature size of the fragment.

2.2.3. Debris Surface-to-Mass Ratio Distribution Model. The surface-to-mass ratio function [13] (probability density) $D_{A/M}$ for debris from $L_c \geq 11cm$ is as in Equation (6). Other sizes are as in Equation (7).

$$\begin{aligned} D_{A/M}(\lambda_c, \chi) = {} & \alpha(\lambda_c)N(\mu_1(\lambda_c), \sigma_1(\lambda_c), \chi) \\ & + (1 - \alpha(\lambda_c))N(\mu_2(\lambda_c), \sigma_2(\lambda_c), \chi), \end{aligned} \quad (6)$$

$$D_{A/M}(\lambda_c, \chi) = N(\mu(\lambda_c), \sigma(\lambda_c), \chi), \quad (7)$$

where $\lambda_c = \lg(L_c)$ is the logarithm of the feature size, the $\chi = \lg(A/M)$ is the logarithm of the surface-to-mass ratio A/M, and its unit is m^2/kg; $N(\mu, \sigma, \chi) = [1/\sigma\sqrt{2\pi}]e^{-(\chi-\mu)^2/2\sigma^2}$ is the normal distribution equation, where μ is the mean, σ is the standard deviation, and $\alpha(\lambda_c) \in [0, 1]$ is the weighting factor associated with λ_c [13].

2.2.4. Debris Velocity Distribution Model. The distribution function of the fragment separation rate from the impact is represented by the following Equation (8).

$$D_{\Delta v}(\chi, \delta) = N(\mu(\chi), \sigma(\chi), \delta), \quad (8)$$

where $\delta = \lg(\Delta v)$ is the logarithm of the separation rate and is the variable of the distribution equation in the unit of m/s;

μ is the mean of the normal distribution function, and $\sigma = 0.4$ is the standard deviation.

2.3. Spacecraft Collision Probability Model with Short-Term Debris Clouds. The time integration algorithm is used to find the collision probability, which applies to a wider range of situations. The time-integration algorithm is described as follows, and the final overall collision probability is derived from the calculation of a single fragment [14]. The mission spacecraft here are assumed to be all Starlink satellites in the same orbit as the target spacecraft, i.e., the threat to all satellites in the same orbit of the constellation from the short-term secondary debris cloud generated by the collision of the target spacecraft with space debris within a certain period is calculated, and the short-term debris cloud is defined as the debris cloud generated for less than half of the mission satellite cycle.

The relationship between the spacecraft's position and velocity and the centre of the debris cloud is shown in Figure 4. Given that the debris probability density is based on the orbital coordinate system with the debris cloud centre as the origin, the motion of the spacecraft is also described

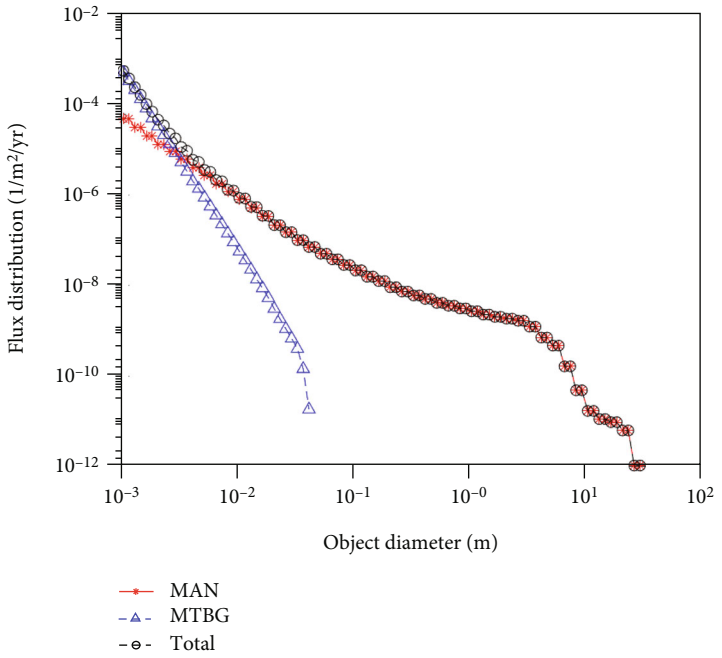

(a) Dimensional characteristics

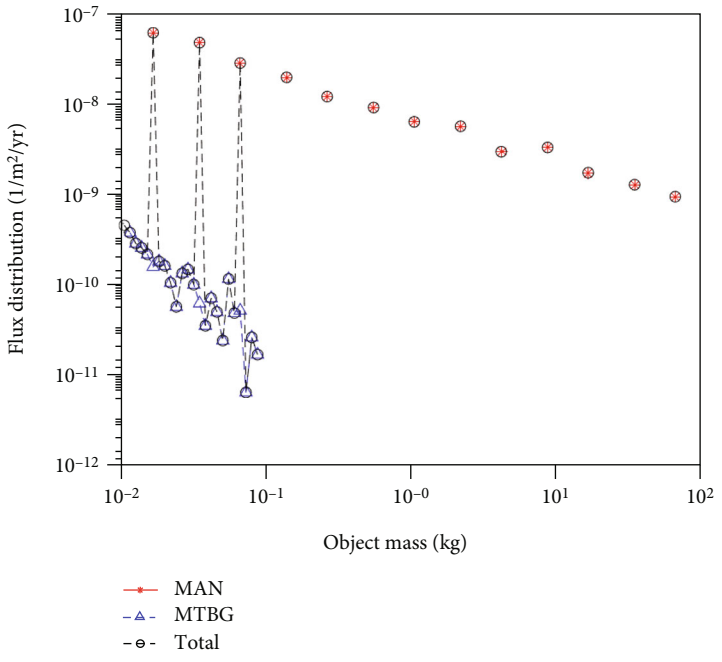

(b) Quality characteristics

Figure 5: Orbital debris flux.

by this coordinate system, as illustrated in the following Equation (9).

$$\begin{bmatrix} R_e(t) \\ V_e(t) \end{bmatrix} = \begin{bmatrix} A(\tau) & B(\tau) \\ C(\tau) & D(\tau) \end{bmatrix} \begin{bmatrix} R_{e0} \\ V_{e0} \end{bmatrix}. \quad (9)$$

$A(\tau), B(\tau), C(\tau), D(\tau)$ is the transfer matrix of relative motion derived from the C-W equation.

The collision probability of a single fragment of the debris cloud with the mission spacecraft at each moment is integrated over time t to obtain the collision probability of the spacecraft with that fragment p_0.

$$p_0 = S\int_{t_0}^{T+t_0} \frac{f\left(B(t)^{-1}R_e(t)\right)\left|D(t)B(t)^{-1}R_e(t) - V_e(t)\right|}{\|B(t)\|}dt, \quad (10)$$

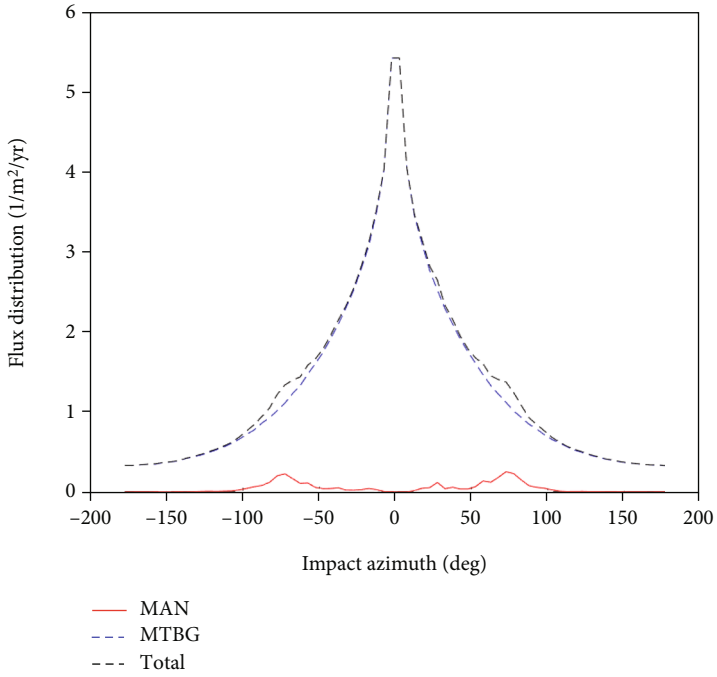

(a) Azimuthal flux

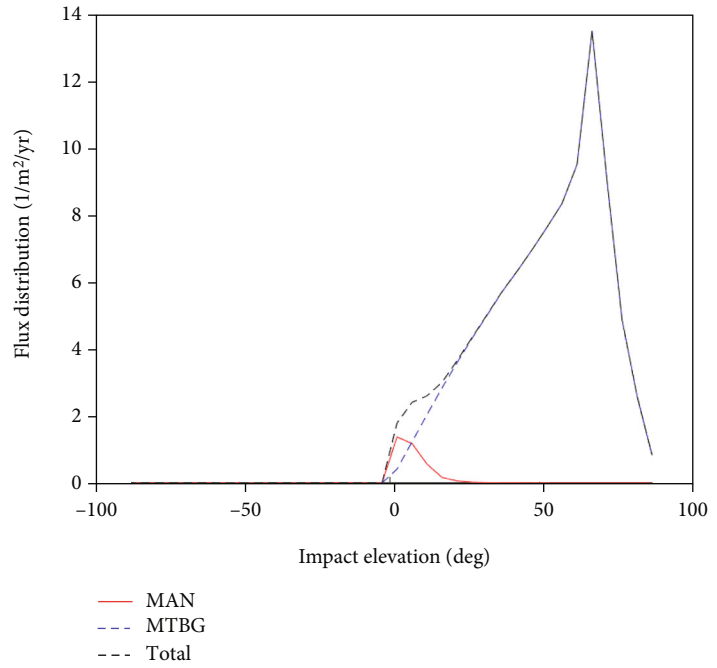

(b) Elevation angle flux

Figure 6: Continued.

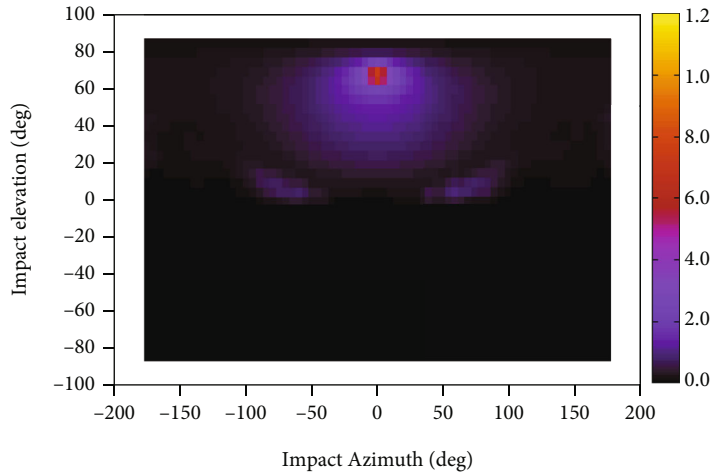

(c) Azimuth and elevation angle distribution heat map

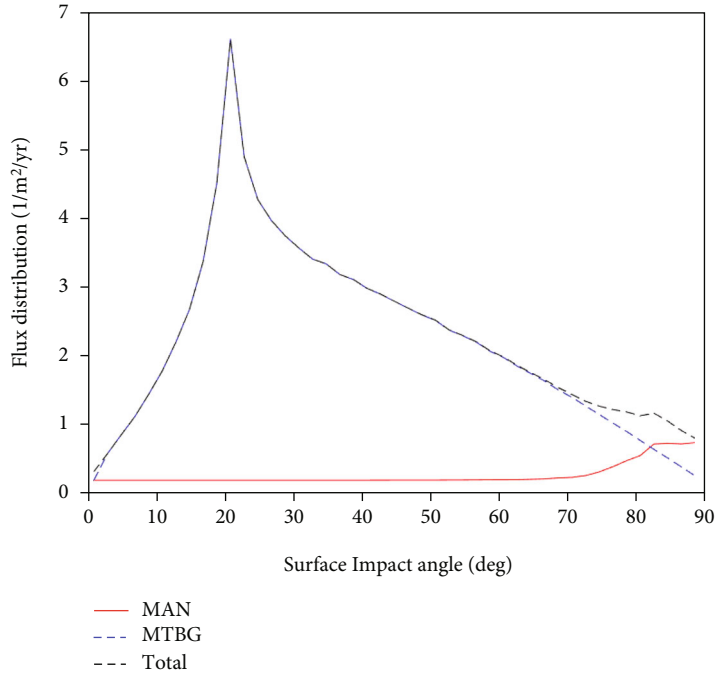

(d) Impact surface angle

Figure 6: Impact angle fluxes calculated from azimuth and elevation angles.

where $V_r(t)$ is the relative rate of debris to the spacecraft in units of m/s, and S is the cross-sectional area of the spacecraft. Figure 4 shows the relative relationship between the satellite and the debris cloud. $R_{e0} = R_e(t_0)$ is the initial displacement of the spacecraft when it enters the debris cloud, $V_{e0} = V_e(t_0)$ is the initial velocity of the spacecraft when it enters the debris cloud, which corresponds to the evolution time of the debris cloud at t_0, $R_e(t) = [r_{ex}, r_{ey}, r_{ez}]^T$ is the displacement of the spacecraft after it enters the debris cloud for $\tau = t - t_0$ seconds, and $V_e(t) = [v_{ex}, v_{ey}, v_{ez}]^T$ is the velocity of the spacecraft after it enters the debris cloud for $\tau = t - t_0$ seconds.

T is the time required for the whole collision process, and to account for the more concentrated debris cloud distribution time and the satellite cycle time, the time T is calculated by 1-30 minutes.

Of all the debris, only those large enough to pose a threat to the spacecraft need to be taken into account. Assuming there are N pieces of "large debris" in the debris cloud, $n = 1, 2, 3, \cdots, N$, the probability of a collision between the spacecraft and k is $p_{N,k}$, i.e., the probability of a collision occurring k out of N large debris is [15]

$$p_k\{X \geq k\} = 1 - \sum_{i=0}^{k-1} p_{N,i}, \quad k = 0, 1, \cdots, N. \tag{11}$$

3. Target Orbital Collision Probability

3.1. Orbital Debris Characteristics. The orbit of Starlink-61 is calculated with a semimajor axis (SMA) of 6886.52 km, an eccentricity ECC) of 0.001511, an inclination (INC) of

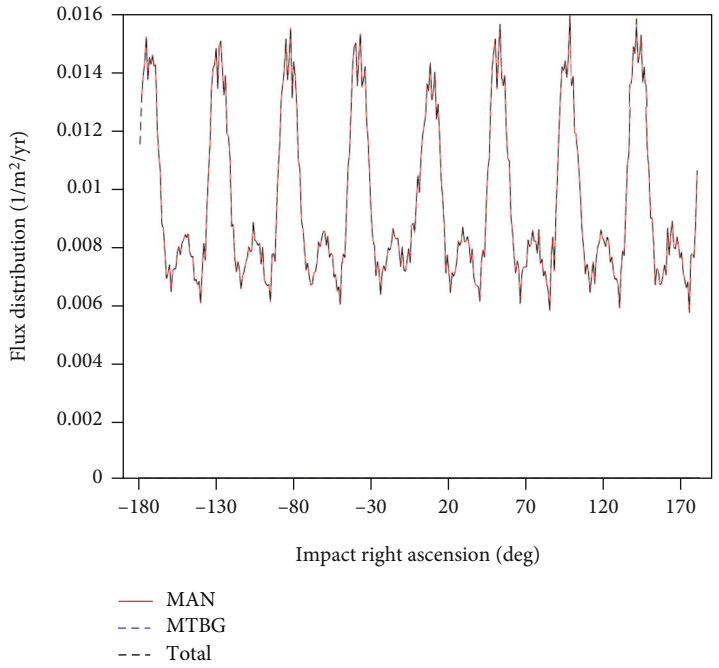

(a) Equatorial meridian

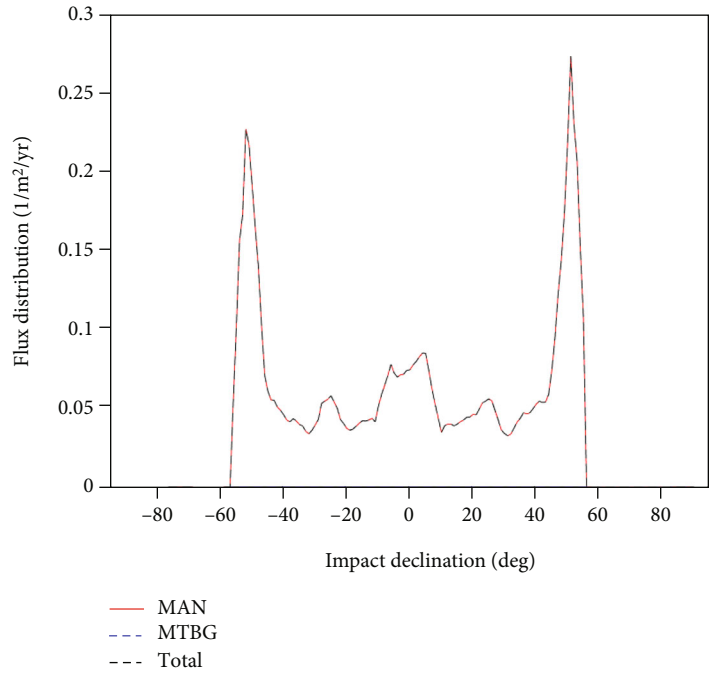

(b) Equatorial latitude

Figure 7: Continued.

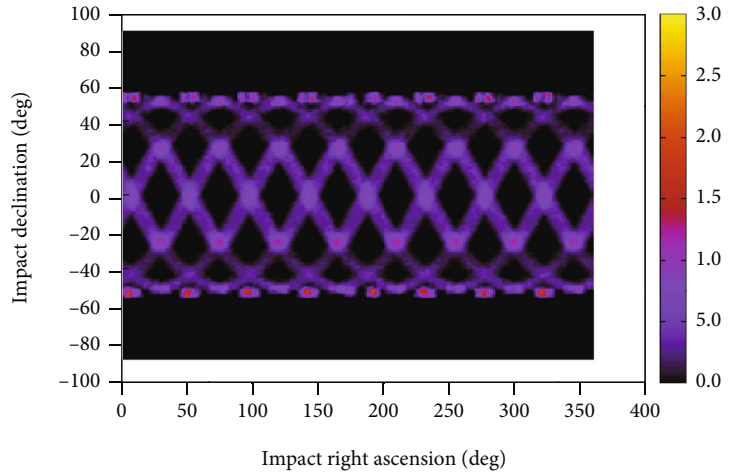

(c) Equatorial latitude and longitude heat map

Figure 7: Longitude fluxes and latitude fluxes at impact sites.

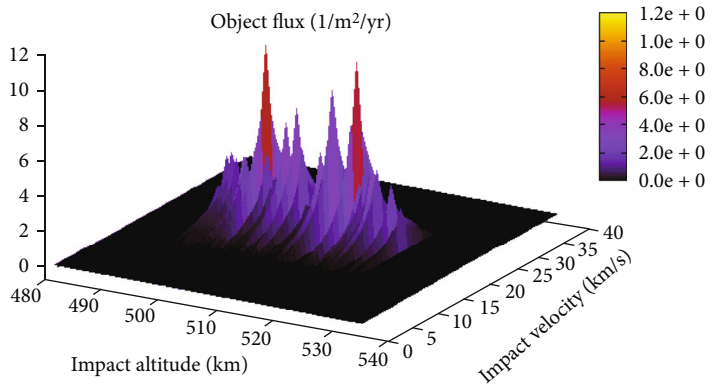

(a) Height flux heat map

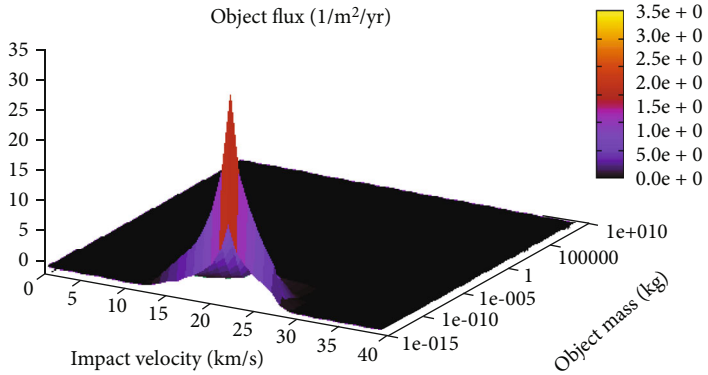

(b) Velocity flux heat map

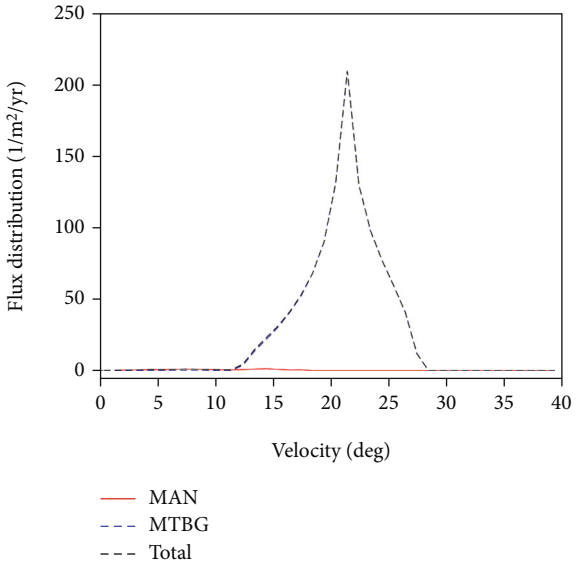

(c) Velocity flux

Figure 8: Fluxes of debris impact height and impact velocity.

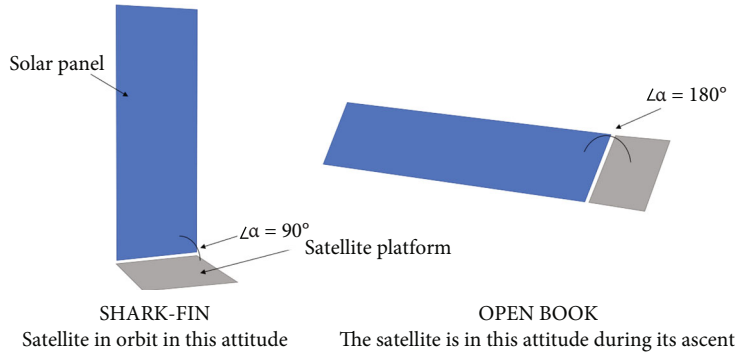

Figure 9: Starlink satellite attitude diagram.

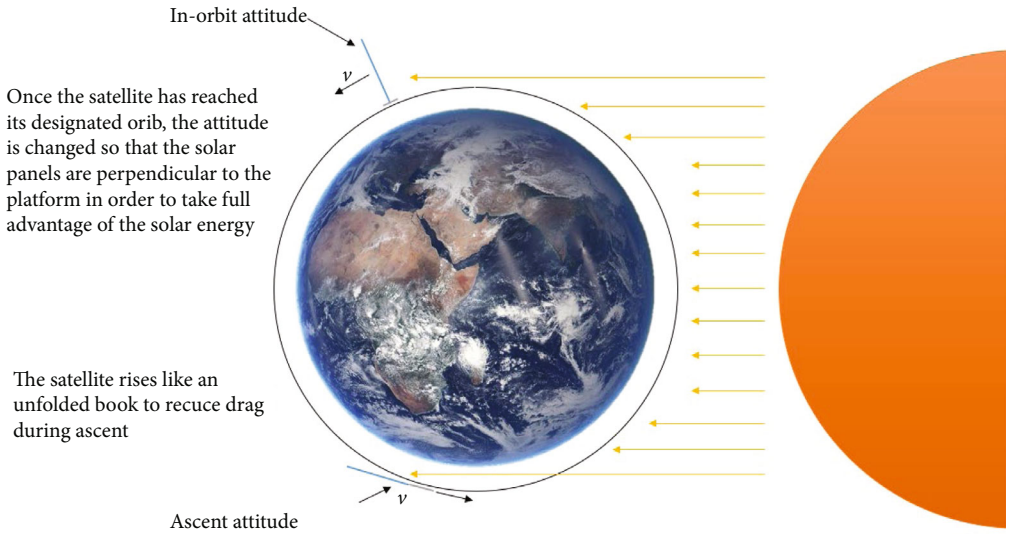

Figure 10: Satellite in-orbit attitude diagram.

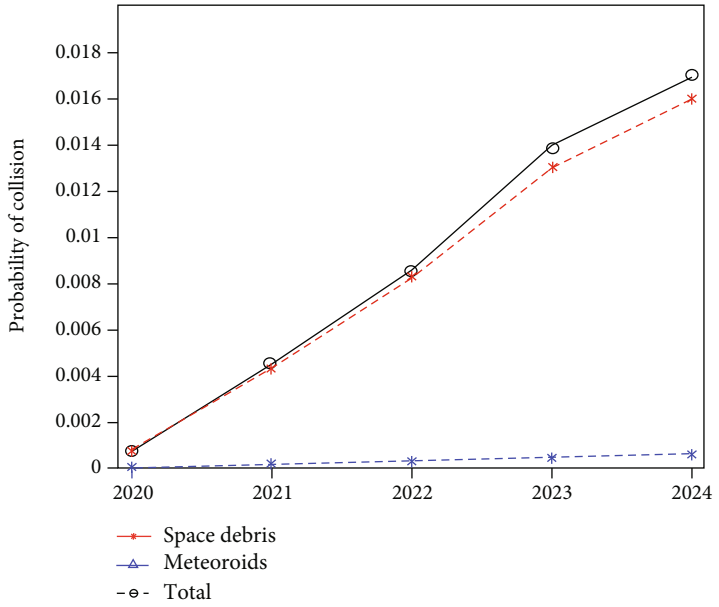

Figure 11: Collision probabilities for all years (space debris represents the collision probability of space debris, and meteoroids represent the collision probability of meteoroids).

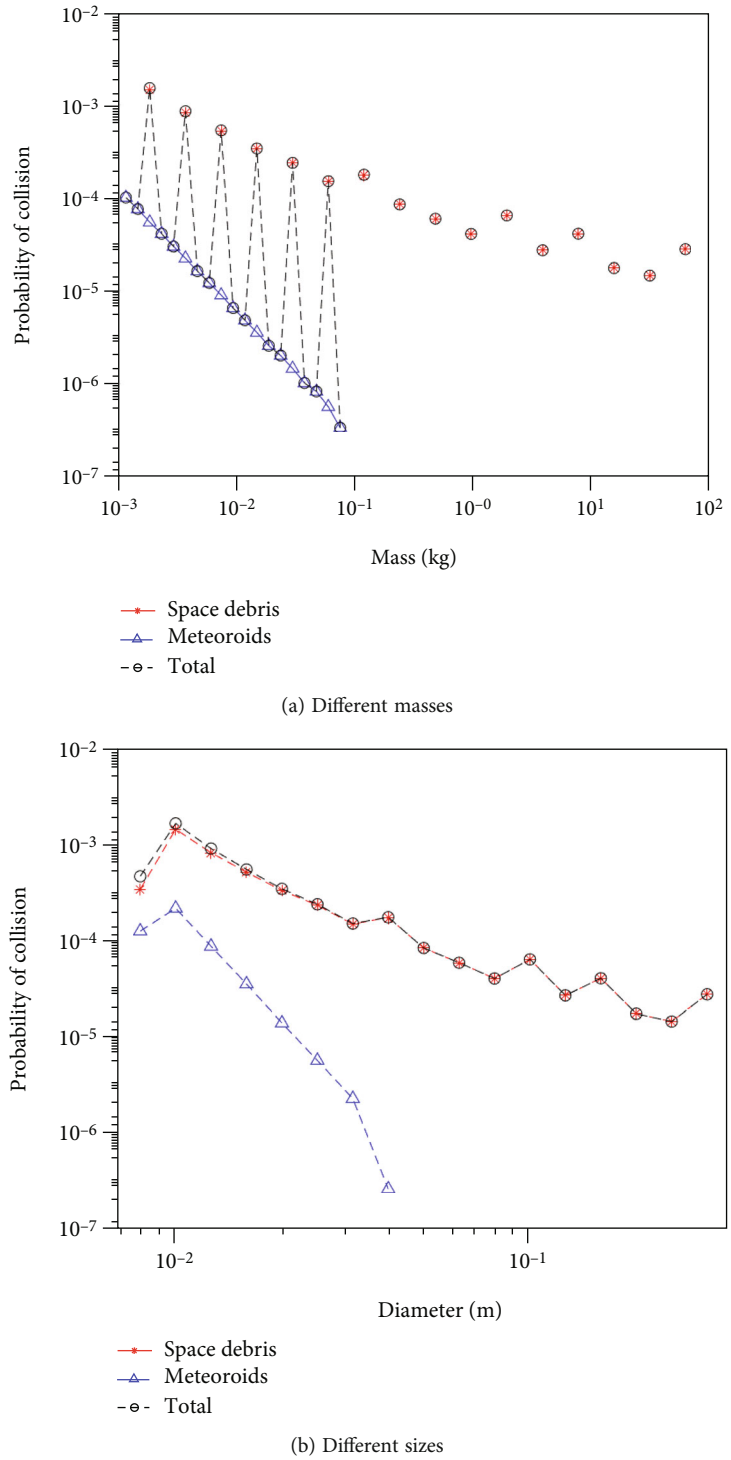

(a) Different masses

(b) Different sizes

Figure 12: The calculation of object collision probability.

53.1385 degrees, a right ascension of ascending node (RAAN) of 102.2289 degrees, and an angle of perigee (AoP) of 28.2438 degrees. And the time period covered by the computation is from 1 November 2020 to 1 November 2024. The debris was extrapolated from the ESA debris extrapolation model MASTER-8 [16].

The debris flux shown in Figure 5 corresponds to the debris size and mass, where MAN denotes man-made, MTBG denotes meteoroid background, and total denotes the sum of the two. The vertical coordinate represents the flux of orbital debris or the passing density [16]. As illustrated in Figure 5(a), the size flux is close to $2.159 \times 10^{-8}/m^2/yr$ for 10 cm fragments and $8.516 \times 10^{-7}/m^2/yr$ for 1 cm fragments, and in Figure 5(b), the mass flux is $2.034 \times 10^{-8}/m^2/yr$ for 0.1 kg space fragments. This paper focuses on the fragments weighing more than 0.1 kg and fragment flux with a diameter

greater than 1 cm. The collision probability calculation for the subsequent collision probability is also primarily concerned with the collision probability of fragments and satellites with these parameters.

The angle of impact also affects the impact effect. Figure 6(a) depicts the impact azimuth angle, which is the smallest at the poles and reaches a maximum of 5.5/m^2/yr at 0 degrees; Figure 6(b) shows the impact elevation angle, which reaches a maximum of 13.5/m^2/yr at 65 degrees; Figure 6(c) represents the heat map of the azimuth and elevation fluxes. The two can determine the surface impact angle that produces the most flow. The surface impact angle flux shown in Figure 6(d) is the greatest at 21 degrees, reaching a maximum of 6.5/m^2/yr at 21 degrees; therefore, it is chosen as the angle input for the collision.

Figure 7 shows the latitude and longitude distribution of the impact site. Based on the latitude, the longitude, and the impact angle, the location of the impact can be calculated. As can be seen from the figure, Figure 7(a) depicts the impact equatorial flux; the equatorial longitude flux is more regular; -180-0 degrees is east longitude; 0-180 degrees is west longitude; the flux at 97.5 degrees west longitude reaches the maximum of 0.01592/m^2/yr. The declination flux at the point of impact is illustrated in Figure 7(b), with the equatorial latitude flux increasing from the equator towards the poles, with a more prominent distribution at both angles and the most prominent flux at 51°N. Figure 7(c) shows a latitude-longitude thermal map of the impact site, with a more regular distribution of impact locations and hotspot locations at higher latitudes.

The collision velocity, as well as the mass and volume velocity of the debris that may collide, is also calculated for the potential collisions, and these factors have a significant impact on whether or not a collision occurs and the outcome of the collision [17]. Figure 8 shows the distribution of fluxes for the target orbital space debris of different velocities, altitudes, and masses, and the fluxes for different velocities upon impact are deduced from the fluxes. The debris impact velocity flux at 21.5 km/s is the highest, reaching 209/m^2/yr.

3.2. Collision Probability. To calculate the probability of a collision induced by the Starlink satellite based on the computed space debris parameters of the target orbit, it is necessary to understand the specific structure of the Starlink satellite, which is composed of a solar panel and a platform body. The specific structure is shown in Figure 9. The satellite is in OPEN BOOK attitude during the ascent, changing to a SHARK-FIN attitude after reaching the designated orbit [18].

In Figure 10, it can be seen that the solar panels are always oriented towards the Sun in order to obtain a greater intensity of solar radiation [18, 20]. The Starlink satellite has three phases of flight: (1) orbital ascent, (2) parking orbit (380 km above the Earth), and (3) in orbit (550 km above the Earth). During orbital ascent, satellites use their thrusters to increase their altitude over a few weeks, when they are in the OPEN BOOK attitude, with some satellites going directly into orbit and others staying in a stalled orbit to allow the satellite to enter another orbital plane. Once the satellites are in working orbit, they reconfigure their antennas so that the antennas face the Earth and the solar arrays move vertically, at which point the satellite is in a SHARK-FIN attitude so that it can track the Sun in order to maximize power generation. The collision analysis in this paper focuses on the state of the satellite after it reaches its working orbit. This attitude occupies most of the satellite's time in orbit, so the satellite can be considered to be in the SHARK-FIN attitude. Figure 10 shows the attitude of the Starlink satellite at different stages with respect to the sunlight [18].

Table 1: Impact point parameters.

Parameter nature	Size
X coordinate of impact point	-3319.90 km
Y-coordinate of impact point	2785.73 km
Z-coordinate of impact point	5351.83 km
Target satellite X-directional subvelocity	0.505 km/s
Target satellite Y-direction subvelocity	-7.450 km/s
Target satellite Z-directional subvelocity	1.447 km/s
Fragment quality	0.1 kg
Fragment X-direction velocity	-0.327 km/s
Fragment Y-direction velocity	4.837 km/s
Fragment Z-direction velocity	-19.4033 km/s
Debris impact angle	21 deg

The attitude change of Starlink satellite in orbit means an increase in the possibility of collision with space debris; hence, the area of the solar panel has a greater impact on the probability of the satellite colliding, according to statistics on DISCOweb [19], and this cross-sectional area is 23.657m^2. In Figure 11, without regard for the size and mass of the collision object, the collision probability increases year by year. While the collision risk mainly comes from space debris, meteoroids have a negligible effect on the collision probability; the total collision probability reaches 0.001 in the first year, far exceeding the red warning threshold of 10^{-4}, and 0.017 in 2024. The collision risk is linearly increasing, with a high probability of catastrophic collisions in the natural operational state and the largely unchanged probability of collisions with meteoroids.

The red warning threshold for space debris collision is 10^{-4} while the yellow warning threshold is 10^{-5}. This paper focuses on the collision probability of debris with the actual energy ratio $\widehat{E}_P \geq \widehat{E}_P^* = 40J/g$, i.e., the collision probability of space debris with the actual energy ratio greater than 40 J/g should be less than the red warning threshold 10^{-4}, so we need to focus on the debris with these parameters [20]. Further calculations are required for the collision probability of debris of varying sizes and masses. Figure 12 shows the probability calculations for the size and mass of the possible collision objects. Among the features of concern, the probability of collision for a fragment of size 1 cm is 0.001681 and for a fragment of mass 0.1 kg is 0.00017692, both exceeding the red warning threshold.

It can be seen that the probability of collision from 10^{-4} kg to 10^{-1} kg exceeds the red warning threshold 10^{-4}, and the probability of collision from 1 kg to 10 kg exceeds the

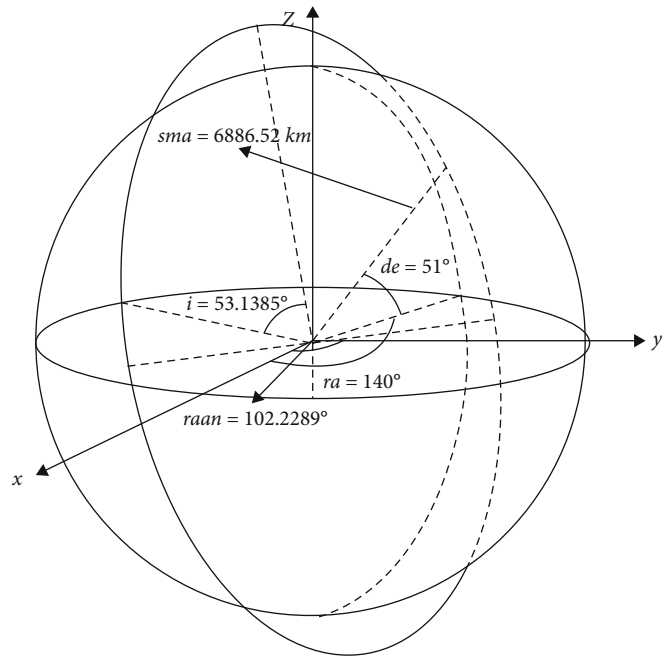

Figure 13: Impact point location.

yellow warning threshold 10^{-5}, indicating that the natural state collision is very likely to occur and collision avoidance control is needed, which provides the basis for the following collision analysis. The fragment mass for the following collision analysis is 0.1 kg [12].

4. Collisional Disintegration and Analysis of Results

4.1. Collision Disintegration State. The debris fluxes and collision probabilities presented above enable the selection of the more salient features of low-orbiting debris and the calculation of the impact of a collision on a Starlink satellite in the target orbit. Based on the data obtained in the previous section, the most likely collision spatial coordinate point is calculated as well as the mass and velocity of the debris colliding at that point and the collision angle. The debris mass is selected according to the red warning threshold 10^{-4}, the debris velocity is taken as 20 km/s, the debris direction vector is shown in Table 1, and the results are obtained as shown in the table below. The disintegration position is converted from the orbital root number to the position in the J2000 coordinate system. The largest flux is the most likely case of collision. The individual parameters of the collision are selected, and Table 1 shows the impact point parameters.

Figure 13 shows the calculated position of the space debris impact point in space. $i = 53.1385°$ indicating the orbital inclination, raan = 102.2289° indicating the orbital ascension declination, de = 51° indicating the impact declination, and ra = 140° indicating the impact declination.

A rough estimate from the disintegration limit $\widehat{E}_P^* = 40J/g$ suggests that debris with a characteristic size larger than 1 cm is a certain threat to the spacecraft and is not considered beyond this range [21]. The impact produces 14088 pieces of debris larger than 1 cm in size.

Figure 14(a) shows the size of the debris cloud and its velocity distribution with most of the debris around 1 cm in size. Figure 14(b) shows the size of the debris cloud and its velocity distribution, with most of the debris masses around 0.0001 kg. The majority of the debris clouds in Figure 15 have surface-to-mass ratios between 0.5-1 m^2/kg and 1-10 m^2/kg, and most of the debris clouds have masses less than 0.5 kg, with the sum of all debris masses being 224.877 kg and an error of 0.934% from the total satellite mass of 227 kg.

Most of the debris masses are concentrated around 0.0001 kg, but there are still a considerable number of debris masses distributed around 0.1 kg, and the debris cloud generated by the impact is believed to pose a significant threat to the safety of the large orbital vicinity. The actual energy ratio distribution of debris is shown in Figure 16(a), and those above the red line are debris with an actual energy ratio exceeding the disintegration limit of 40 J/g. The final result is shown in Figure 16(b), and there are 9996 debris not exceeding the disintegration limit and 4092 debris exceeding the disintegration limit.

Figure 17 depicts a fragmentation and mass and speed distribution, which shows the speed distribution for various fragmentation qualities and sizes, while Figure 18 is the distribution of fragmentation speed. It can be seen from the figure that the velocity of the debris cloud is concentrated in the 3-8 km/s range, with the mass of less than 0.5 kg being the most massive and the mass greater than 10 kg falling between 0 km/s and 8 km/s. Most of the 0.5 kg-1 kg fragments can exceed 40 J/g, posing a threat to satellites. The fragments of this quality range are distributed over all speeds, and almost all high-speed debris ($V > 10$ km/s) are

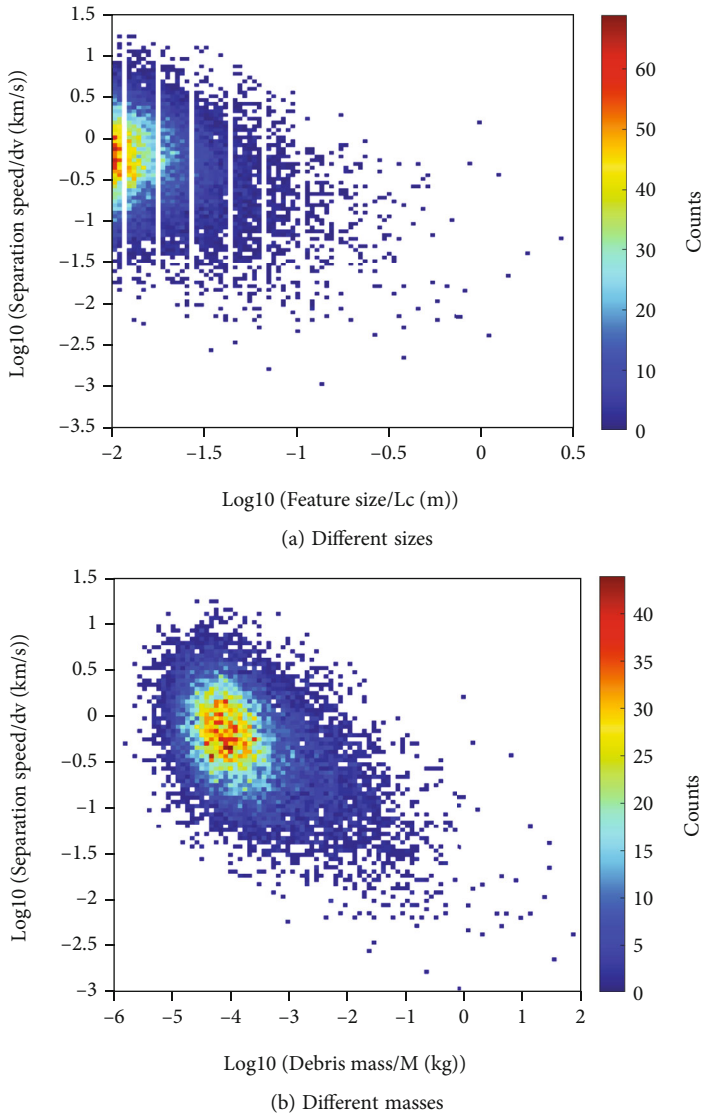

Figure 14: Impact debris separation rate-characteristic size distribution and impact debris separation rate-debris mass distribution.

about 1 kg. The fragments that need to be considered are referred to by their actual energy ratio, and the subsequent collision probability calculation is dependent on the actual energy ratio.

Among the debris cloud formed by the disintegration of the target satellite, 4092 pieces of debris can affect the mission satellite (the same orbiting satellite of the constellation). Because the mega constellation satellites are very dense, there is a high possibility of secondary collision; as for the short-term debris cloud generated by one collision, it is necessary to calculate the probability of the short-term debris cloud colliding with the mission satellite and calculate the probability of secondary collision, to assess the risk of a secondary collision.

4.2. Collision Probability of Short-Term Debris Clouds with Coorbiting Spacecraft. The orbital true proximity angle of the same orbital mission satellite is 48.56°, and the other orbital roots are the same as those of the disintegrated target satellite. Figure 19 shows the collision probability between the short-term debris cloud and the mission spacecraft with time. The collision probability between the debris cloud and the satellite at 15 min is already higher than the red warning threshold 10^{-4}, and with the extension of time, the collision probability climbs rapidly. When the Starlink satellite collides with orbital debris, the resulting short-term debris cloud may collide with the same orbiting satellite within a short period, making it difficult to adjust the orbit for avoidance and control. This means that when a Starlink satellite collides with orbital debris, the resulting short-term debris cloud will threaten other satellites.

5. Conclusion

This paper investigates the possibility of collisions between Starlink satellites and space debris, as well as the mass, size, velocity, impact point location, and impact angle of space debris at Starlink orbital altitude. After the collision, a

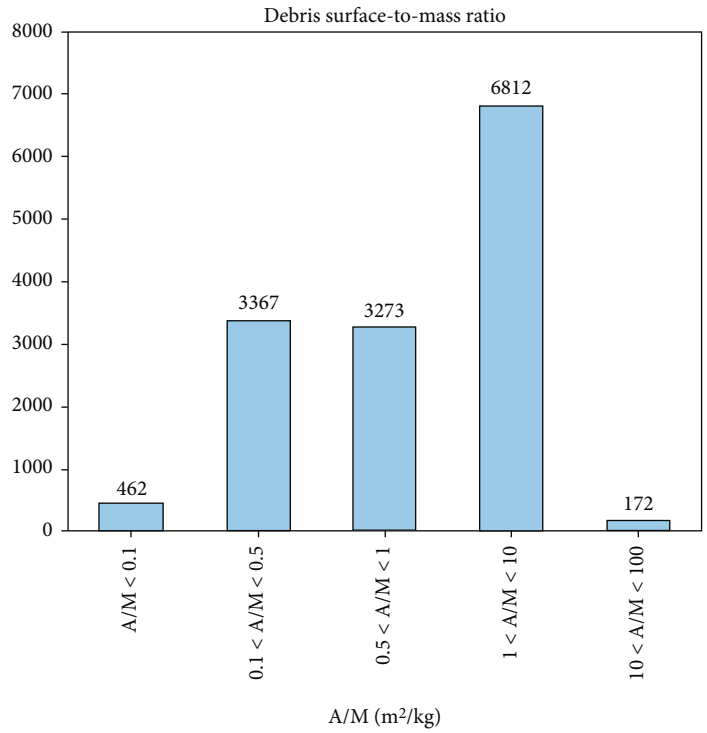

(a) Debris surface-to-mass ratio

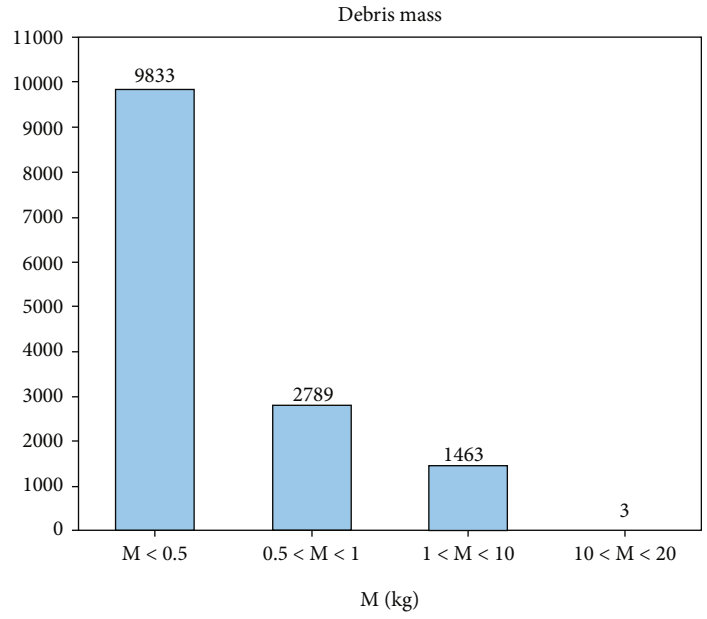

(b) Debris mass

Figure 15: Fragment surface-to-mass ratio and fragment mass.

short-term debris cloud will be generated, posing an inevitable collision risk to the satellite in the same orbit, i.e., secondary collision. The probability of collision between the short-term debris cloud and the Starlink satellite in the same orbit is examined, and the following conclusions are drawn.

(1) The mass flux, size flux, velocity flux, longitude and latitude flux of the impact point, and angular flux of space debris impacting the target satellite's orbit are obtained. The collision probability of space debris with Starlink satellite is obtained, it is found that the collision probability increases linearly year by year, and the collision probability of the target satellite with debris weighing more than 0.1 kg or larger than 1 cm exceeds the red alert threshold of collision 10^{-4}

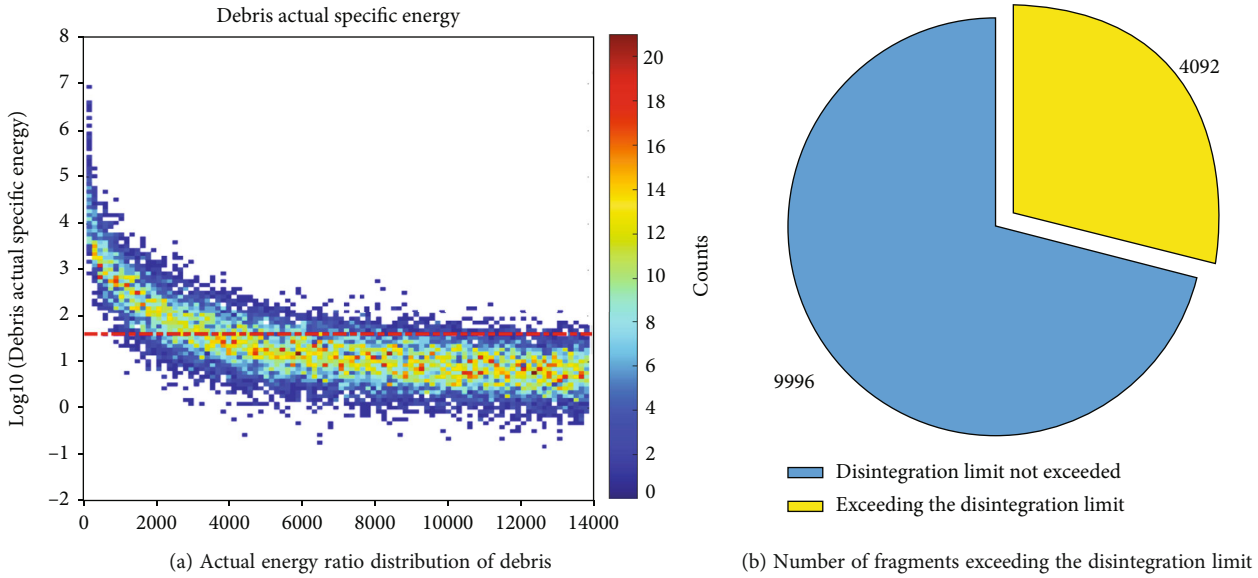

(a) Actual energy ratio distribution of debris

(b) Number of fragments exceeding the disintegration limit

Figure 16: The actual energy ratio of debris.

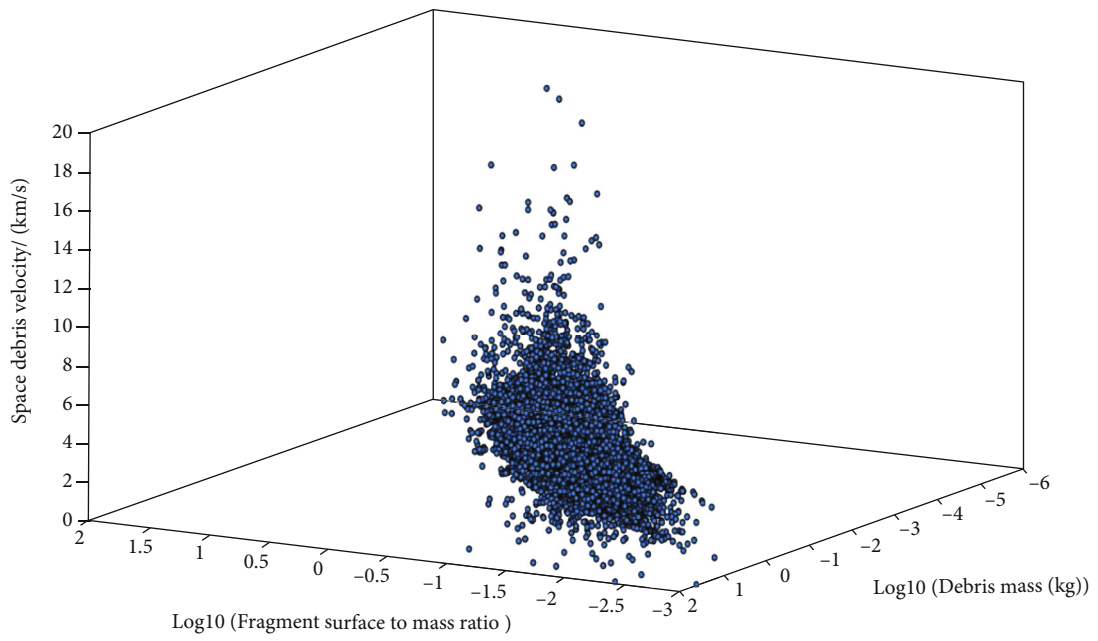

Figure 17: Surface-to-mass ratio and velocity distribution.

(2) The collision scenario is simulated, and statistics on the short-term debris cloud are gathered, including mass distribution, surface-to-mass ratio distribution, size distribution, velocity distribution, and the actual energy ratio distribution of the debris, and a total of 4092 debris causing the threat are identified. The probability of collision between a satellite in the same orbit and a short-term debris cloud within 30 minutes is calculated. The probability of collision between the debris cloud and the target satellite exceeds the red warning threshold of 10^{-4} at 15 minutes and reaches 2.0915×10^{-4} at 30 minutes. Starlink satellites may cause secondary collisions, jeopardising the normal operation of the same orbit or even the whole constellation

Due to the existence of mega constellations in the future low orbit space, the probability of collision between constellation satellites and space debris is already quite high, but the chain collision caused by the secondary collision will be a greater threat to space safety, necessitating further research into ways to avoid and control secondary collisions.

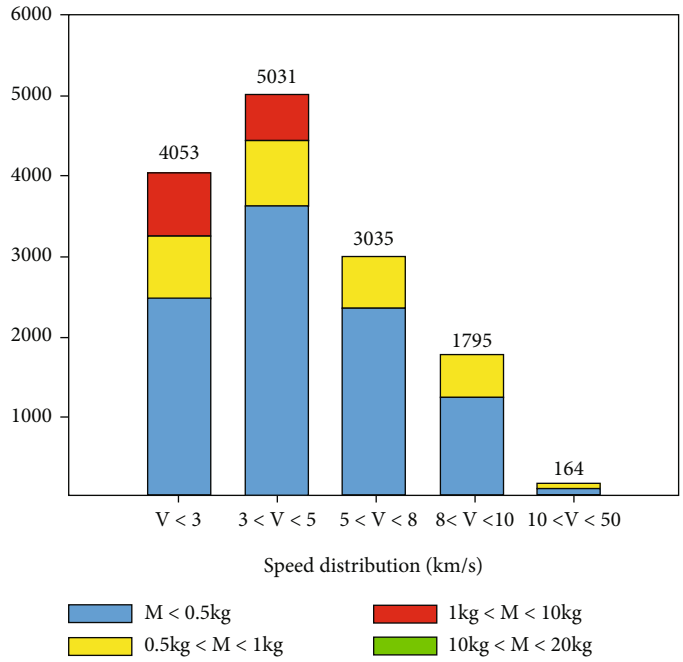

Figure 18: Debris velocity distribution.

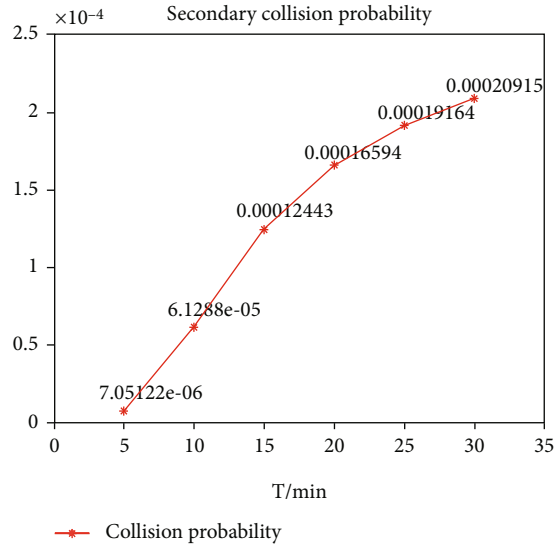

Figure 19: Secondary collision probability.

Satellite orbital transfer often requires warning and calculation of orbital transfer plans, and orbital transfer cannot be performed in time to avoid the sudden generation of short-term debris clouds. Therefore, if a collision occurs in one of the Starlink constellation's satellites, it will threaten the operational safety of satellites in the same orbit or even nearby orbits. It is proposed that future studies need to extend this effect to the whole constellation and investigate the effect of secondary collisions on the entire Starlink satellites that occur within a short period when a collision is generated by the resulting debris cloud.

Data Availability

The data are available in the link "https://discosweb.esoc.esa.int/objects/59334 and https://celestrak.com."

Conflicts of Interest

The authors declare that they have no conflicts of interest.

References

[1] Jeff, "foust. FCC approves Starlink license modification," 2021, https://spacenews.com/fcc-approves-Starlink-license-modification/.

[2] j. radtke, c. kebschull, and e. stoll, "Interactions of the space debris environment with mega constellations-using the example of the OneWeb constellation," *Acta Astronautica*, vol. 131, pp. 55–68, 2017.

[3] V. Braun, A. Lüpken, S. Flegel et al., "Active debris removal of multiple priority targets," *Advances in Space Research*, vol. 51, no. 9, pp. 1638–1648, 2013.

[4] Jeff, "foust. ESA spacecraft dodges potential collision with Starlink satellite," 2019, https://spacenews.com/esa-spacecraft-dodges-potential-collision-with-Starlink-satellite/.

[5] "Aroged. Chinese space station nearly collided with Starlink satellites twice-Chinese unleashed their wrath on musk," 2021, https://www.aroged.com/2021/12/27/chinese-space-station-nearly-collided-with-Starlink-satellites-twice-chinese-unleashed-their-wrath-on-musk/.

[6] L. J-C, N. L. Johnson, and N. M. Hill, "Controlling the growth of future LEO debris populations with active debris removal," *Acta Astronautica*, vol. 66, no. 5-6, pp. 648–653, 2010.

[7] J. Drmola and T. Hubik, "Kessler syndrome: system dynamics model," *Space Policy*, vol. 44-45, pp. 29–39, 2018.

[8] CelesTrakhttps://celestrak.com/.

[9] L. Anselmo and C. Pardini, "Dimensional and scale analysis applied to the preliminary assessment of the environmental criticality of large constellations in LEO," *Acta Astronautica*, vol. 158, article S0094576517309694, 2017.

[10] A. C. Boley and M. Byers, "Satellite mega-constellations create risks in low Earth orbit, the atmosphere and on Earth," *Scientific Reports*, vol. 11, no. 1, article 10642, 2021.

[11] A. Ellery, "Tutorial review of bio-inspired approaches to robotic manipulation for space debris salvage," *Biomimetics*, vol. 5, no. 2, p. 19, 2020.

[12] H. Shen, W. Wang, and L. Yiyong, *Spacecraft Space Impact Modeling and Analysis*, Science Press, 2014.

[13] N. Cimmino, G. Isoletta, R. Opromolla et al., "Tuning of NASA standard breakup model for fragmentation events modelling," *Aerospace*, vol. 8, no. 7, p. 185, 2021.

[14] J. L. Forshaw, G. S. Aglietti, S. Fellowes et al., "The active space debris removal mission Remove Debris. Part 1: from concept to launch," *Acta Astronautica*, vol. 168, pp. 293–309, 2020.

[15] P. Zhao, J. Liu, and C. C. Wu, *Chenchen WU*, vol. 63, no. 11, 2020, Survey on research and development of on-orbit active debris removal methods, Science China Technological Sciences, 2020.

[16] V. Braun, Q. Funke, S. Lemmens, and S. Sanvido, "DRAMA 3.0- upgrade of ESA's debris risk assessment and mitigation analysis tool suite - Science Direct," *Journal of Space Safety Engineering*, vol. 7, no. 3, pp. 206–212, 2020.

[17] H. Klinkrad, J. R. Alarcon, and N. Sanchez, *Collision Avoidance for Operational ESA Satellites*, 2005.

[18] SpaceXhttp://www.spacex.com/.

[19] "Starlink 43-DISCOSweb," https://discosweb.esoc.esa.int/objects/59334.

[20] N. Adil, P. J. Alexander, and B. M. Cunningham, "An economic "Kessler Syndrome": a dynamic model of earth orbit debris," *Economics Letters*, vol. 166, pp. 79–82, 2018.

[21] J. C. Liou, "An active debris removal parametric study for LEO environment remediation," *Advances in Space Research*, vol. 47, no. 11, pp. 1865–1876, 2011.